# Oculomotor Plant Characteristics: The Effects of Environment and Stimulus

Oleg Komogortsev, *Member*, *IEEE,* Alexey Karpov, *Member*, *IEEE*,
and Corey Holland, *Student Member*, *IEEE*

***Abstract*—This paper presents an objective evaluation of the effects of environmental factors, such as stimulus presentation and eye tracking specifications, on the biometric accuracy of oculomotor plant characteristic (OPC) biometrics. The study examines the largest known dataset for eye movement biometrics, with eye movements recorded from 323 subjects over multiple sessions. Six spatial precision tiers (0.01°, 0.11°, 0.21°, 0.31°, 0.41°, 0.51°), six temporal resolution tiers (1000 Hz, 500 Hz, 250 Hz, 120 Hz, 75 Hz, 30 Hz), and three stimulus types (horizontal, random, textual) are evaluated to identify acceptable conditions under which to collect eye movement data. The results suggest the use of eye tracking equipment providing at least 0.01° spatial precision and 30 Hz sampling rate for biometric purposes, and the use of a horizontal pattern stimulus when using the two-dimensional oculomotor plant model developed by Komogortsev et al. [1].**

***Index Terms*—Biometrics, eye movements, mathematical modeling, pattern analysis, security and protection.**

## I. Introduction

THE HUMAN FACE is one of the most distinctive features with which we assign and recognize identity in our daily lives, and its overall structure is largely dependent on the physical structure of the human visual system. Facial geometry was first proposed as a biometric trait in the 1960s [2], but did not begin to gain traction with the biometric community until the 1990s [3]. Early research in this area was highly susceptible to aging effects [4, 5] and environmental factors [6], such as angle and lighting; however, recent developments have made significant progress in eliminating these issues [7].

Today, there are many techniques for performing facial recognition, which may be broadly described by two categories: those that compare geometric features of the face, and those that compare statistical features of the image [8]. Techniques in the former category, such as elastic bunch graph matching [9], typically model salient features of the face, such as the nose, mouth, and eyes; while techniques in the latter category, such as tensor factorization [7], apply mathematical transformations and analysis to the individual pixels of the facial image.

Fingerprints are often regarded as the gold standard of biometric accuracy [8], with open dataset competitions showing equal error rates approaching 2% under the effects of skin distortion and rotation [10]; however, fingerprint biometrics suffer from two major drawbacks. First, and most notably, fingerprints are easy to forge; and while fingerprints provide substantial resistance to zero-effort attacks, it takes minimal effort to defeat such a system [11]. Second, fingerprint biometrics are intrusive; that is, in order for biometric features to be collected, an individual must physically interact with the biometric sensor.

Speculation about the identifying characteristics of iris patterns can be traced as far back as the late 1800s [12], but was largely ignored in a biometric context until the 1980s, when a patent [13] stifled innovation for nearly a decade. The study of iris pattern biometrics picked up quickly however [14], and was achieving authentication accuracies that rival fingerprints [10] by the early 2000s [15]. Unfortunately, like fingerprints, iris pattern biometrics are easily fooled by minimal-effort attacks [16].

Much of the current work in this area is based on the principles of Daugman's research [17], in which the iris pattern is projected onto a Gabor wavelet, and compared with a test for statistical independence. Often it is necessary to correct for orientation and occlusions, but even still these techniques are highly efficient, with computation times measurable in milliseconds on modern hardware [18].

Over the past decade, study of the human visual system has shown that eye movements may be utilized to uniquely identify individuals in a biometric context [19, 20]. Consisting of both physical and neurological components [21], and due to the minute scale, the accurate replication of eye movements outside of a living subject is practically infeasible, providing inherent levels of counterfeit-resistance and liveness detection that many traditional biometrics cannot [22].

Further, eye movements may be captured and processed in real-time using an unmodified camera [23] through the use of modern video-oculography techniques. Not only does this make the collection of eye movement data inexpensive and

Manuscript received June 8, 16. This work is supported in part by NSF CAREER Grant #CNS-1250718 and NSF GRFP Grant #DGE-11444666, and NIST Grant #60NANB15D325. Special gratitude is expressed to Katie Holland for her aid with technical illustrations.

O. Komogortsev is with the Computer Science Department, Texas State University, San Marcos, TX 78666 USA (phone: 512-245-0349; fax: 512-245-8750; e-mail: ok11@txstate.edu).

A. Karpov is with the Computer Science Department, Texas State University, San Marcos, TX 78666 USA (e-mail: ak26@txstate.edu).

C. Holland is with the Computer Science Department, Texas State University, San Marcos, TX 78666 USA (e-mail: ch1570@txstate.edu).

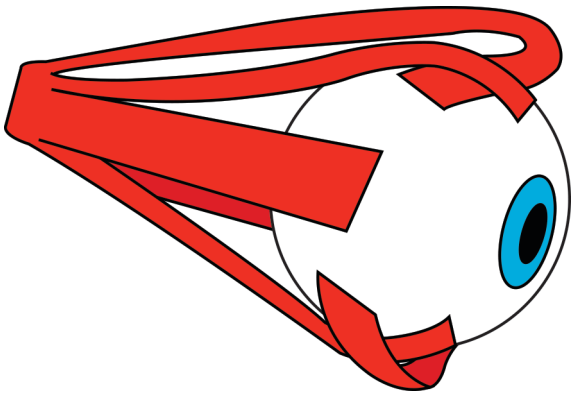

Figure 1. The oculomotor plant.

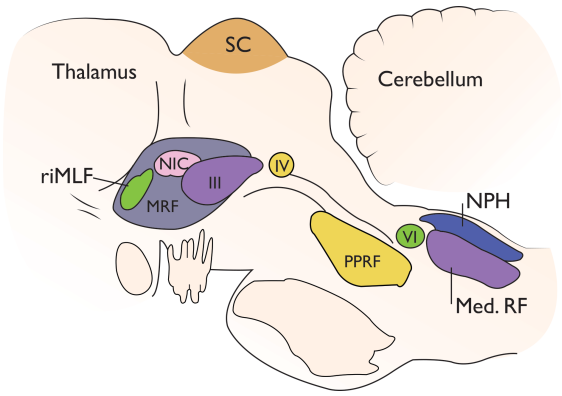


Figure 2. The brainstem control.

efficient, but the ability to capture iris patterns and eye movements with a single sensor allows for easy integration into multi-model biometric systems.

Biometrics traits may be distinguished by their invariance and persistence. The invariance of eye movements was established in early experiments by Noton and Stark [25], in which it was identified that the eye movements produced by a subject during the initial viewing of a pattern were repeated during 65% of subsequent viewings. The persistence of eye movements has been established in many short-term studies, described in Section I.B; however, as a relatively recent addition to the biometric field, with initial investigations beginning in 2004, there are currently no longitudinal studies that establish the long-term persistence of eye movements.

### A. *Human Visual System*

The human visual system is composed of the oculomotor plant, shown in Figure 1, and brainstem control, shown in Figure 2. The oculomotor plant [21] describes the major physical components of the human visual system, including the eye globe, six extraocular muscles, surrounding tissues, ligaments, tendon-like components, and viscous fluids; and the brainstem control [24] describes the major neurological components of the human visual system, including sub-regions of the thalamus, superior colliculus, and posterior parietal cortex.

The brainstem control generates a neural signal to each of the extraocular muscles that corresponds to the type, direction, and magnitude of eye movement, and the oculomotor plant responds, enacting the mechanical functions that produce the movement. In concert, these systems produce six basic types of eye movement [21], including: fixation, saccade, smooth pursuit, vestibulo-ocular reflex, optokinetic reflex, and vergence/version.

Fixation occurs when the eye is held in a relatively stable position to provide visual acuity on a fixed object; saccades occur when the eye rotates rapidly between points of fixation, with little visual acuity maintained during rotation; smooth pursuit occurs when the eye rotates slowly, maintaining fixation on a slowly moving object; optokinetic reflex refers to the sequence of smooth pursuits and saccades which occur when the eye attempts to maintain fixation on a rapidly moving object; vestibulo-ocular reflex refers to the corrective eye movements that occur to maintain fixation on a stationary object during head movement; and vergence/version refers to the corrective eye movements that occur to maintain fixation on an object whose distance changes. These may be further divided into a number of sub-types, such as micro-fixations and express saccades [21].

### B. *Previous Research*

The foundations of eye movement biometrics stem from early research in scanpath theory, where the term scanpath refers to the spatial path formed by an ordered sequence of fixations and saccades. In 1971, Noton and Stark [25] found that the scanpath formed by a subject during the initial viewing of a pattern was repeated in 65% of subsequent viewings. Further, it has been found by various sources that the scanpath produced for a given stimulus pattern tends to vary from person to person [25-27]. These inherent properties of scanpath—subconscious reproduction, variation by subject, and variation by stimulus—provide a basis for the use of eye movements as a behavioral biometric.

In 2004, Kasprowski and Ober [20] were the first to examine the use of eye movements in a biometric context. Utilizing voice recognition techniques, the first 15 cepstral coefficients were extracted from the positional eye movement signal, with information fusion by Bayes classifiers, C4.5 decision trees, polynomial SVMs, and KNN ($k$ = 3 and $k$ = 7). With a subject pool of 9 participants, the described techniques achieved an average 1% false acceptance rate and 23% false rejection rate.

In 2005, Bednarik et al. [28] examined a set of pupil-related features, including: pupil diameter, distance between corneal reflections, gaze velocity, and change in pupil diameter over time, using Fourier transfer and PCA to reduce the continuous signal to a feature vector, with information fusion by weighted sum. With a subject pool of 12 participants, the described techniques achieved a 92% rank-1 identification rate using leave-one-out cross-validation.

In 2006, Silver and Biggs [29] examined a range of high-level eye movement features, including: coordinates and duration of the 8 longest fixations, fixation count, average fixation duration, average saccade velocity, average saccade duration, and average vertical position, using KNN as a distance function with information fusion by a probabilistic neural network. With a subject pool of 21 participants, the described techniques achieved an average 66% true positive rate and 98% true negative rate.

In 2011, Holland and Komogortsev [30] examined a set of high-level average and aggregate eye movement features (CEM-P), including: fixation count, average fixation duration, average saccade amplitude, average saccade velocity, average saccade peak velocity, velocity waveform indicator, scanpath length, scanpath area, regions of interest, inflection count, amplitude-duration coefficient, and main sequence coefficient, using a Gaussian distance function, with information fusion by weighted mean. With a subject pool of 32 participants, the described techniques achieved a 22% equal error rate.

In 2012, Komogortsev et al. [31] examined the use of mathematical models of the oculomotor plant to extract the physical properties of the human visual system from the observable properties of eye movements (OPC). Biometric features included a number of anatomical parameters, with information fusion by Hotelling's $T^2$ test. With a subject pool of 59 participants, the described techniques achieved a 19% minimum half-total error rate.

In 2013, Komogortsev and Holland [32] examined a set of high-level features related to corrective eye movements (COB), including: multiple types of saccadic dysmetria and express saccades, with information fusion by likelihood ratio, linear SVM, and random forest. With a subject pool of 32 participants, the described techniques achieved 25% equal error rate and 47% rank-1 identification rate.

Most recently, Holland and Komogortsev [19] examined a set of low-level features based on the distribution of basic eye movements throughout a recording (CEM-B). Distributions of fixations and saccades were compared using the two-sample Cramér von-Mises test, with information fusion by 50-tree random forest. With a subject pool of 32 participants, the described techniques achieved 17% equal error rate and 83% rank-1 identification rate.

### C. Motivation & Hypothesis

Eye movements present a novel and unique solution to the challenges faced by modern biometrics. Consisting of both physical and neurological components, and due to the minute scale, the accurate replication of eye movements outside of a living subject is practically infeasible (if not impossible), providing an inherent level of liveness detection and counterfeit-resistance. Further, recent advances in video-oculography allow for the efficient capture of eye movements from even low-quality image sensors, reducing the cost of entry and enabling integration with many existing iris, periocular, and facial recognition systems.

In this paper, we hypothesize that environmental factors, such as stimulus and eye tracking specification may affect the biometric accuracy of oculomotor plant characteristics (OPC), and that the effects of these environmental factors may differ from existing studies of alternative eye movement biometrics, such as CEM-P [30] and CEM-B [19]. The current paper expands greatly on our previous research by: examining a substantially larger pool of 323 subjects and exploring the effects of spatial precision, sampling rate, and stimulus presentation on oculomotor plant characteristics (OPC).

## II. Oculomotor Plant Characteristics

The biometric techniques investigated in this paper are based on the oculomotor plant characteristic (OPC) techniques originally proposed by Komogortsev et al. [31]. An oculomotor plant model describes the physical structure of the human visual system as a series of equations. Muscle parameters, referred to as oculomotor plant characteristics (OPC), are estimated from the eye movement recording to produce a model that accurately represents the eye movements of a given individual. The estimated OPC values provide a biometric template that can be used for authentication.

### A. Oculomotor Plant Model

There are a variety of models that have been proposed to simulate the mechanics of the human visual system [33], typically representing the oculomotor plant as a linear one-dimensional model or a non-linear three-dimensional model. Despite decades of research, as far back as the 1970s [34], there does not yet exist a perfect mathematical representation of the human visual system, due largely to the complexity of the neurological components involved. For our purposes, an oculomotor plant model was selected to allow accurate reproduction of two-dimensional human eye movements within certain limitations, while accounting for expected anatomical properties of the human visual system.

The current work focuses on a two-dimensional linear homeomorphic model of the oculomotor plant, developed by Komogortsev et al. [1] as an extension of Bahill's one-dimensional model [35]. The considered model sacrifices some accuracy for computational tractability, while still accounting for major anatomical components. Further, the model is particularly suited for parallel computation, as the horizontal and vertical components of eye movement can be modeled separately.

### B. Oculomotor Plant Characteristics

We refer to the parameters of the oculomotor plant model as oculomotor plant characteristics (OPC), which describe the physical and neurological properties of the human visual system. The considered model, derived and explained in [1, 36] has 18 parameters for each direction of movement (in this case, horizontal and vertical):

1. *Series Elasticity* (AG) [$K_{AG\_SE} = 2.5$ g/°]
2. *Series Elasticity* (ANT) [$K_{ANT\_SE} = 2.5$ g/°]
3. *Length-Tension Relationship* (AG) [$K_{AG\_LT} = 1.2$ g/°]
4. *Length-Tension Relationship* (ANT) [$K_{ANT\_LT} = 1.2$ g/°]
5. *Force-Velocity Relationship* (AG) [$B_{AG} = 0.046$ g×s/°]
6. *Force-Velocity Relationship* (ANT) [$B_{ANT} = 0.022$ g×s/°]
7. *Passive Viscosity* [$B_P = 0.06$ g×s/°]
8. *Tension Slope* (AG) [$N_{AG\_C} = 0.8$ g]
9. *Tension Slope* (ANT) [$N_{ANT\_C} = 0.5$ g]
10. *Inertial Mass* [$J = 0.000043$ g×s$^2$/°]
11. *Activation Time* (AG) [$\tau_{AG\_AC} = 11.7$]
12. *Activation Time* (ANT) [$\tau_{ANT\_AC} = 2.4$]
13. *Deactivation Time* (AG) [$\tau_{AG\_DE} = 2.0$]
14. *Deactivation Time* (ANT) [$\tau_{ANT\_DE} = 1.9$]
15. *Tension Intercept* [$N_{FIX\_C} = 14.0$ g]
16. *Neural Pulse* (AG) [$N_{AG\_SAC} = 55$ g]
17. *Neural Pulse* (ANT) [$N_{ANT\_SAC} = 0.5$ g]

18. *Neural Pulse Width* [PW = 6 ms]

The terms AG and ANT refer to agonist and antagonist muscles respectively, where the agonist muscle contracts to rotate the eye globe and the antagonist muscle expands to resist the pull of the agonist, with bracketed terms indicating default parameter values. Values in square brackets represent default model parameters used in the OPC biometric template computation procedure discussed later.

Series elasticity describes the resistive properties of the extraocular muscles, associated with tendons. The length-tension relationship describes the relationship between the length of the muscle and the force it is capable of exerting. The force-velocity relationship describes the relationship between the velocity of muscle contraction and the force it is capable of exerting. The tension slope and tension intercept describe the reaction of the muscle to innervation and ensure equilibrium during fixation, respectively. As well, the inertial mass of the eye globe and passive viscosity of the surrounding tissue must be accounted for.

The considered model employs a pulse-step representation of the neuronal control signal, in which the pulse represents the magnitude of the firing rate of neurons during saccade and the step represents the magnitude during fixation. The pulse width indicates the duration of the neural pulse, which cannot exceed the duration of the saccade, and requires at least 3 ms for activation/deactivation at the beginning and end of a saccade. Activation and deactivation time describe the time required for changes in the neuronal control signal to propagate through the extraocular muscles.

### C. Estimation of Oculomotor Plant Characteristics

The most time-consuming part of OPC-based authentication is the estimation of oculomotor plant characteristics from recorded saccade trajectories, shown in Figure 3. Parameter estimation seeks to identify the OPC parameters that minimize the difference between the recorded saccade trajectory and the simulated trajectory produced by the model.

The estimation routine utilizes the Nelder-Mead simplex search algorithm for multi-dimensional unconstrained non-linear minimization [37]. A vector of OPC parameters is initialized with realistic default values based on the relevant literature [35, 38, 39]. An error function invokes the oculomotor plant model to simulate a saccadic trajectory for a given set of OPC parameters, and returns the absolute difference between the measured and simulated trajectories. The Nelder-Mead simplex algorithm adjusts the vector of OPC parameters, shrinking or expanding the search region for each parameter, in an attempt to minimize the result of the error function, until some exit criteria is satisfied.

Constraints are imposed on the OPC vector to reduce the search space and prevent unrealistic parameter values. OPC parameter values are not allowed to vary by more than an order of magnitude above or below the default value, and the stability of the model is taken into account when accepting an optimized OPC parameter vector.

### D. Software Performance

The OPC estimation software was originally implemented in MATLAB, utilizing the features of the Parallel Computing Toolbox to off-load computation to a parallel compute cluster.

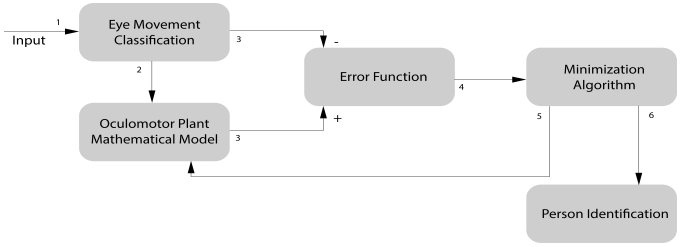


Figure 3. OPC estimation procedure.

In this way, a control program handles communication with MATLAB workers in the compute cluster, and each worker runs the OPC estimation routine on its subset of trajectories.

While this software scales almost linearly with the number of parallel workers, the cost of additional cluster nodes and MATLAB licenses makes this solution less than desirable. As an alternative, the OPC estimation routine was re-written with NVIDIA's CUDA technology to take advantage of the massively parallel computation capabilities of modern GPUs.

In this way, the Nelder-Mead simplex algorithm executes on the CPU, while the oculomotor plant model simulates saccade trajectories on the GPU. Komogortsev et al. [36] two-dimensional oculomotor plant model is particularly suited for this type of application, as it can be easily expressed as a set of matrix equations, taking advantage of the fact that many GPU devices have been optimized for matrix operations.

Since sending and retrieving data from the GPU is more expensive than standard memory access, measured saccade trajectories are loaded into GPU memory once at the start of execution, reducing the overhead of potentially sending each saccade trajectory individually. The Nelder-Mead simplex algorithm is initialized on the CPU, and an initial set of OPC parameters is sent to the GPU. Model simulation and the error function are executed on the GPU, and the error is returned to the Nelder-Mead algorithm, which tests for exit criteria and provides a new set of OPC parameters to the GPU.

The employed CUDA solution benchmarked on a single NVIDIA GeForce GTX 460, with 336 CUDA cores, is approximately 400% faster than the entire 64-node MATLAB cluster, with 2.53 GHz Intel Xeon E5540 processors. Considering there are now graphics cards with more than 5000 cores (for example, the GeForce GTX TITAN Z) and faster clock rates, and that multiple graphics cards may be connected to work as a single unit, it is likely that in the future a CUDA solution will allow real-time OPC estimation for live OPC-based biometric systems. Please note that detailed technical description of the CUDA solution is beyond the scope of this paper and will be discussed in a separate manuscript.

## III. Methodology

Eye movement recordings employed in this paper were collected as part of an NSF CAREER grant study, and will be made available online for public use within the next year. A segment of the dataset is provided as a part of the BioEye 2015 competition, available at: www.bioeye.info.

### A. Participants

Eye movement data was collected for a total of 335 subjects (178 males, 157 females), ages 19 – 46 with an average age of

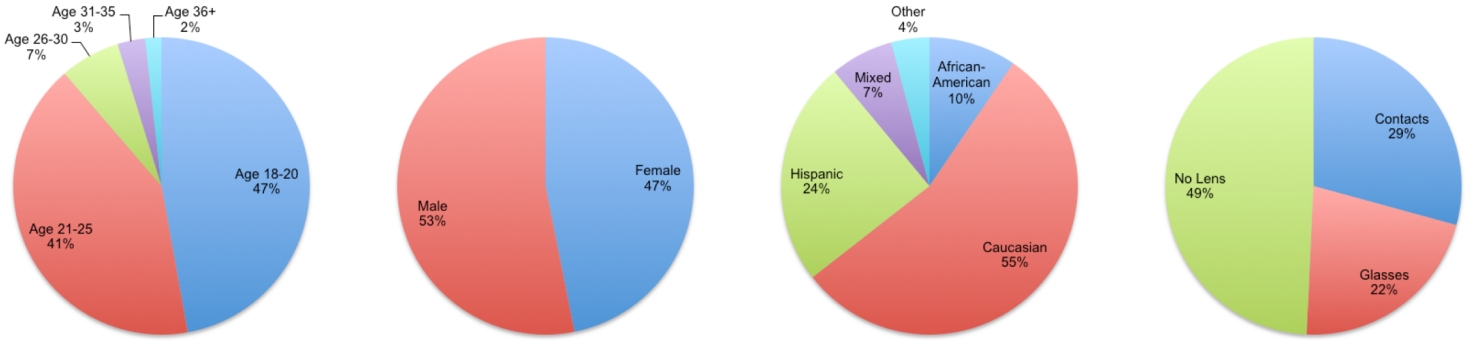


Figure 4. Demographic breakdown of participants by age, gender, ethnicity, and vision.

22 (SD = 4), with demographics summarized in Figure 4. 322 of the subjects performed 2 recordings for each stimulus, 1 of the subjects performed 1 recording for each stimulus, and 12 of the subjects were unable to produce usable recordings, for a total of 645 unique eye movement recordings per stimulus, with an inter-session interval between each type of stimulus of approximately 20 minutes. The inter-session interval was selected to reduce variability in recordings, and may not reflect real-world conditions. Texas State University's institutional review board approved the study, and subjects provided informed consent.

For the 12 subjects that failed to produce usable recordings, these subjects were unable to proceed through eye tracking calibration, and never progressed to the point of stimulus recording. This can occur for various reasons, including: excessive eye moisture, squinting, and shape or color of the eye. For more details on conditions that might lead to failed calibration, see [40].

### B. *Apparatus & Software*

Eye movements were recorded using an EyeLink 1000 eye tracking system [41], with a sampling rate of 1000 Hz, vendor-reported spatial precision of 0.01°, vendor-reported spatial accuracy of 0.5°, average calibration accuracy of 0.5° (SD = 0.2°), and average data validity of 97% (SD = 5%). Note, the EyeLink 1000 vendor refers to spatial precision as spatial resolution [42]; however, we have confirmed with the vendor that this is identical to the definition of spatial precision given in the current paper. Stimuli were presented on a flat screen monitor positioned at a distance of 550 millimeters, with dimensions of 474×297 millimeters, and screen resolution of 1680×1050 pixels. A chin rest was employed to improve stability. All algorithms and analysis were implemented and performed in MATLAB, and executed using a 4.0 GHz quad-core CPU with 16 GB memory.

### C. *Procedure*

Eye movement recordings were generated for three distinct stimulus patterns (horizontal, random, and textual) under closely controlled conditions, in an attempt to achieve the best possible baseline accuracy. This included restrictions to head mobility and inter-session intervals that may not accurately reflect real-world usage. While such restrictions limit the usability of such a system, there exist a wide range of eye tracking systems with differing levels of spatial precision, sampling rate, and available mobility. It is expected that the results presented in the current paper will aid future research in selecting appropriate systems.

Eye movement recordings were parsed and processed to remove invalid data points. Recordings were stored in an eye movement database, with each record linked to the stimulus, subject, and session that generated the recording. Dithering and downsampling were applied (exclusively) to the eye movement recordings to artificially reduce spatial precision and sampling rate for the best performing stimulus. The recordings were then classified into fixations and saccades using an eye movement classification algorithm [43].

A velocity threshold algorithm (I-VT) with documented accuracy [44] was employed to classify individual data points with a velocity greater than 20°/sec as belonging to a saccade, with all remaining points belonging to fixations. A micro-saccade filter re-classified saccades with amplitude less than 0.5° as fixations, followed by a micro-fixation filter which re-classified fixations with a duration less than 100 milliseconds as saccades. Saccades of less than 4° amplitude were rejected in order to omit micro-saccades and corrective saccades from analysis, as these saccadic sub-types exhibit different behavior than normal saccades. Saccades with duration less than 20 milliseconds were rejected to omit potential artifacts caused by blinks and provide more uniform data quality. OPC parameters were estimated for the horizontal component of each remaining saccade, the vertical component was discarded to reduce computation time, according to the techniques described in Section II.

Eye movement recordings were partitioned into training and testing sets, by subject, according to a uniformly random distribution; such that, all recordings from half of the subject pool of a given dataset appeared in the training set, with the other half of the subject pool in the testing set, and there was no subject overlap between training and testing sets. Error rates were calculated under biometric verification and identification scenarios for 20 random partitions of training and testing sets. Regression was performed on the error rates achieved across all partitions to generate receiver operating characteristics (false acceptance rate vs. true positive rate) and cumulative match characteristic (rank vs. identification rate) curves, with $R^2 > 0.95$ in all cases. Equal error rate, rank-1 identification rate, and area-under-curve were calculated from the regression.

Biometric match scores were generated comparing OPC parameters between pairs of recordings. Each recording generated a set of 18-parameter OPC vectors for each saccade, these vectors were compared between recordings using Hotelling's $T^2$ test. Error rates were then calculated on the testing set for individual matches under biometric verification and identification scenarios.

Biometric verification involves comparing each record in the testing set against every other record in the testing set exactly once [8]. False acceptance rate is defined as the rate at which imposter match scores exceed the acceptance threshold, false rejection rate is defined as the rate at which genuine match scores fall below the acceptance threshold, and true positive rate is defined as the rate at which genuine match scores exceed the acceptance threshold. The equal error rate is the rate at which false acceptance rate and false rejection rate are equal. The receiver operating characteristic (ROC) plots true positive rate against false acceptance rate, and the area-under-curve of the ROC provides a metric by which to compare the accuracy achieved by ROC curves.

Biometric identification involves comparing every record in the testing set against every other record in the testing set, with identification rates calculated from the largest match score(s) in each comparison set [8]. Identification rate is defined as the rate at which enrolled subjects are successfully identified as the correct individual, where rank-*k* identification rate is the rate at which the correct individual is found within the top *k* matches. Then, the rank-1 identification rate is the rate at which the correct individual has the highest match score. The cumulative match characteristic (CMC) plots identification rate by rank, for all ranks, and the area-under-curve of the CMC provides a metric by which to compare the accuracy achieved by CMC curves.

### D. Stimulus Patterns

The horizontal pattern stimulus (HOR) made use of a technique typically employed in eye movement research to evoke a fixed-amplitude horizontal saccade at regular intervals [21]. A small white circle sized 0.58° with a black dot in the center sized 0.3° to facilitate accurate fixation jumped back and forth across a plain black background, eliciting a saccade for each jump. The distance between jumps was set to correspond to 30° of the visual angle, due in part to screen constraints, complications separating low-amplitude saccades (less than 1°), and variation in the dynamics of high-amplitude saccades (greater than 50°). Subjects were instructed to follow the white circle with their eyes, with 100 horizontal saccades elicited per session, and 2 recording sessions per subject.

The random pattern stimulus (RAN) was similar in presentation to the horizontal pattern stimulus. A small white circle with the same properties as the horizontal stimulus jumped across a plain black background in a uniformly distributed random pattern, eliciting a saccade for each jump. Subjects were instructed to follow the white dot with their eyes, with 100 randomly directed oblique saccades elicited per session, and 2 recording sessions per subject. The random pattern stimulus is an important use case for biometrics, as it is more resistant to relay spoof attacks; and, unlike the horizontal and textual stimuli, the random stimulus is largely immune to learning effects that may degrade the biometric sample over time.

The textual pattern stimulus (TEX) made use of various excerpts from Lewis Carroll's "The Hunting of the Snark." The poem was chosen for its difficulty and nonsensical content, forcing readers to progress slowly and carefully through the text. Textual excerpts were selected to ensure that reading required approximately 1 minute, line lengths and the difficulty of material was consistent, and learning effects did not impact subsequent readings. Subjects were given different textual excerpts for each recording session, with 2 recording sessions per subject.

It must be noted that the recordings for horizontal, random, and textual stimuli were part of a larger experiment in which subjects watched various types of stimulus. The total duration of all stimuli and periods of rest did not exceed one hour.

## IV. Results

For each experiment, records were partitioned into training and testing sets by subject, according to a uniformly random distribution. With half of the subject pool in the training set, and half of the subject pool in the testing set, without overlap. Algorithm parameters were selected on the training set and regression was performed on biometric error rates of the testing set over 20 random partitions.

### A. The Effects of Stimulus Type

To examine the effects of stimulus on biometric accuracy, three different stimulus patterns (described in the previous section) were presented to each subject. Eye movements were recorded for the horizontal, random, and textual stimulus patterns, each of which exercises different aspects of the human visual system. In the case of the random stimulus, we have included results from the horizontal (H) and vertical (V) components of movement for comparison. As was noted previously, the remaining stimuli analyzed only the horizontal component of movement. For biometric verification, Figure 5 provides equal error rates and area-under-curve for ROC curves. For biometric identification, Figure 6 provides rank-1 identification rates and area-under-curve for CMC curves.

The horizontal stimulus had a clear advantage in terms of biometric accuracy. The random stimulus exhibited the worst identification accuracy, whereas the textual stimulus exhibited the worst verification accuracy. In the case of the textual stimulus, this is likely due to the fact that eye movements during a reading task tend towards relatively low-amplitude saccades, which are known to have certain characteristics such as waveform which differ from large-amplitude saccades [21].

In the case of the random stimulus, which induces a large number of oblique saccades, we hypothesize that the lower biometric accuracy may be caused by a combination of component stretching and higher amplitude saccades. First, oblique saccades are affected by component stretching [45], the process by which the velocity of the lower-amplitude component of a two-dimensional saccade is reduced such that both components have a similar duration. Synchronization issues in the neuronal control signal of the horizontal and vertical components of movement during stretching can manifest in the complex shapes of oblique saccades [46],

which are difficult to model. Further, there are multiple theories on the specifics of how component stretching occurs in humans [47]. Without a clear consensus on the underlying mechanism for component stretching, the oculomotor plant model ignores the effects of component stretching during modeling and employs a simplified pulse-step neuronal control signal, which may lead to reduced biometric accuracy when modeling oblique saccades.

Second, saccades of larger amplitudes cannot be modeled as accurately by the chosen oculomotor plant model due to simplifications made to increase computational tractability, specifically: 1) the model employs a linear representation of fundamentally non-linear anatomical components; and 2) three-dimensional rotational movements are modeled as two-dimensional translations. Saccades of smaller amplitudes can be accurately modeled despite these assumptions, but error introduced by these simplifications compounds as the amplitude of the saccade increases.

When considering the horizontal and vertical components of movement extracted from the random stimulus, it can be seen in Figure 5 that the horizontal component yields lower equal error rates and higher rank-1 identification rates than the vertical component. This may be explained by the fact that vertical eye movements are affected by four extraocular muscles (superior recti, inferior recti, superior oblique, and inferior oblique), while the oculomotor plant model only accounts for two (superior and inferior recti). In comparison, the horizontal component is only affected by two extraocular muscles (lateral and medial recti), and similarly represented by two muscles in the model. The simplified representation of the vertical component reduces the accuracy of the applied model and may be responsible for the overall reduction in biometric accuracy.

It should be noted that information fusion of biometrics for both horizontal and vertical components can provide better performance than either; however, the investigation of this performance is beyond the scope of the current paper.

### B. *The Effects of Spatial Precision*

Spatial precision represents variance in the positional accuracy of the recorded eye movement signal and is measured by equation (3) presented in [48]. Spatial precision is an important measure of eye tracking quality and is affected by multiple factors [48].

To examine the effects of spatial precision on biometric accuracy, dithering was applied to recordings for the textual stimulus prior to eye movement classification. Dithering reduced baseline precision by adding uniformly distributed error to the recorded eye movement position; considered spatial precision tiers from a hardware base of 0.01° include: 0.01°, 0.11°, 0.21°, 0.31°, 0.41°, and 0.51°. In other words, a spatial precision of 0.11° implies 0.1° of random noise. For biometric verification, Figure 7 provides equal error rates and area-under-curve for ROC curves. For biometric identification, Figure 8 provides rank-1 identification rates and area-under-curve for CMC curves.

In both verification and identification scenarios, there is an almost exponential loss of biometric accuracy as spatial precision is reduced. In fact, the relative 69% increase in equal error rate (from 14.5% to 24.5% EER) and the relative 333% reduction in rank-1 identification rate (from 24.7% to 7.4% IR) when spatial precision is reduced from the baseline 0.01° to 0.11° suggests that, in its current state, OPC-based biometrics are very sensitive to precision degradation and that precision should be maintained at a low level for OPC-based biometrics to achieve the best possible accuracy.

### C. *The Effects of Sampling Rate*

To examine the effects of sampling rate on biometric accuracy, downsampling was applied to recordings for the textual stimulus prior to eye movement classification. Downsampling reduced the sampling rate by removing data points to lower the average time between points; considered sampling rate tiers from a hardware base of 1000 Hz include: 1000 Hz, 500 Hz, 250 Hz, 120 Hz, 75 Hz, and 30 Hz. For biometric verification, Figure 9 provides equal error rates and area-under-curve for ROC curves. For biometric identification, Figure 10 provides rank-1 identification rates and area-under-curve for CMC curves.

In both scenarios, sampling rate appears to have very little effect on biometric accuracy, with a slight linear trend as sampling rate is reduced. Biometric verification accuracy varies by roughly 2% equal error rate in terms of the absolute difference from sampling rates of 120 Hz to 1000 Hz, and biometric identification accuracy varies by roughly 3% identification rate in terms of the absolute difference from sampling rates of 75 Hz to 500 Hz, with a noticeable jump at 1000 Hz. Based on these results, sampling rate should be considered secondary to spatial precision when selecting an eye tracking system for OPC-based biometrics.

### D. *The Effects of Scaling*

To examine the impact of scaling on the estimation of biometric accuracy, error rates were calculated on subsets of the total subject pool for the textual stimulus. Subsets of the subject pool were selected randomly according to a uniform distribution, without regard for factors such as race, gender, or age; considered subject pools included: 50, 100, 150, 200, 250, 300, and 335 subjects. For biometric verification, Figure 11 provides equal error rates and area-under-curve for ROC curves. For biometric identification, Figure 12 provides rank-1 identification rates and area-under-curve for CMC curves.

In terms of verification accuracy, there was no discernable difference in equal error rates produced for a subject pool of 50 or a subject pool of 323; this result is mirrored by the area-under-curve. In the case of identification, there was a slight reduction in rank-1 identification rates as the subject pool increases. As the subject pool increases, the random chance probability of the correct subject having the highest match score is reduced. For example, with 2 subjects, the random chance that the correct subject has the highest match score is 50%, and with 100 subjects, the random chance that the correct subject has the highest match score is 1%. With this in mind, the 36% rank-1 identification rate with 50 subjects is comparable to the 25% rank-1 identification rate with 323 subjects. This is further supported by the fact that the area-under-curve of the cumulative match characteristic depicted in Figures 11 and 12 was highly stable from 50 subjects to 323 subjects, and in fact increased from 93% to 94% as the size of the subject pool increased.

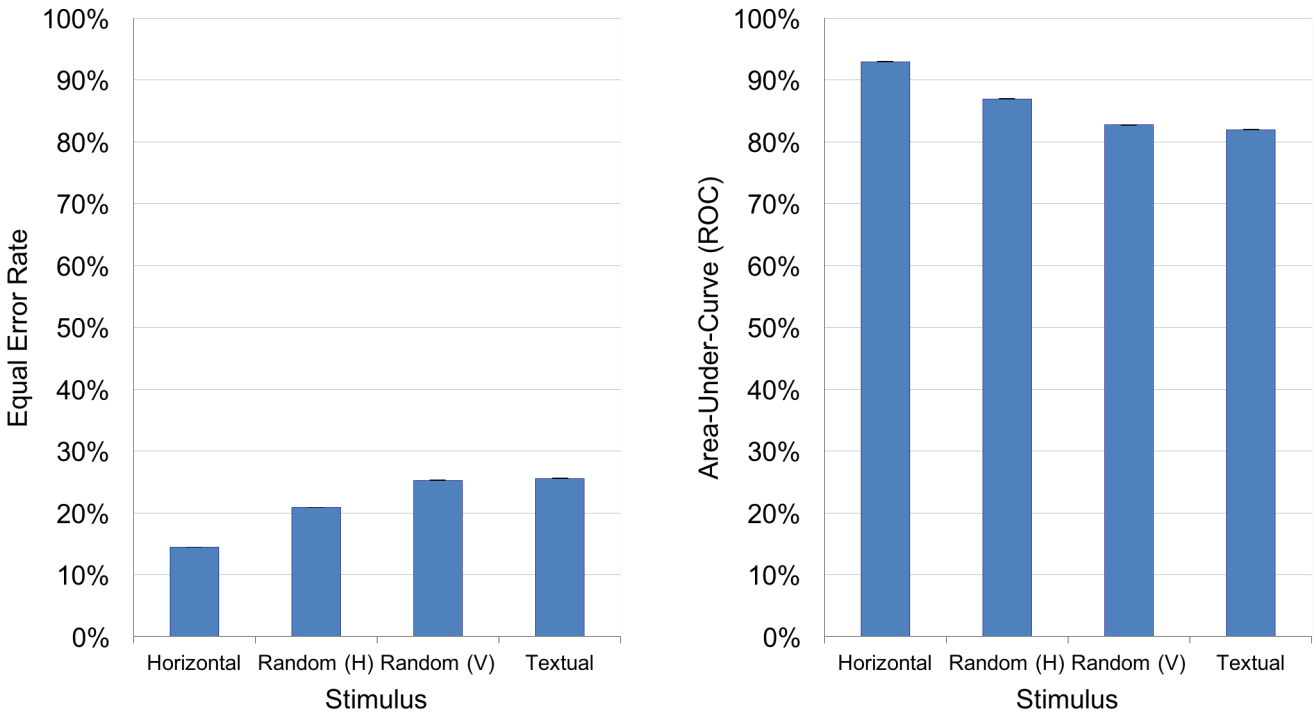


Figure 5. The effects of stimulus type on the biometric accuracy of eye movements in a verification scenario. Error bars indicate 95% confidence interval for the regression of error rates.

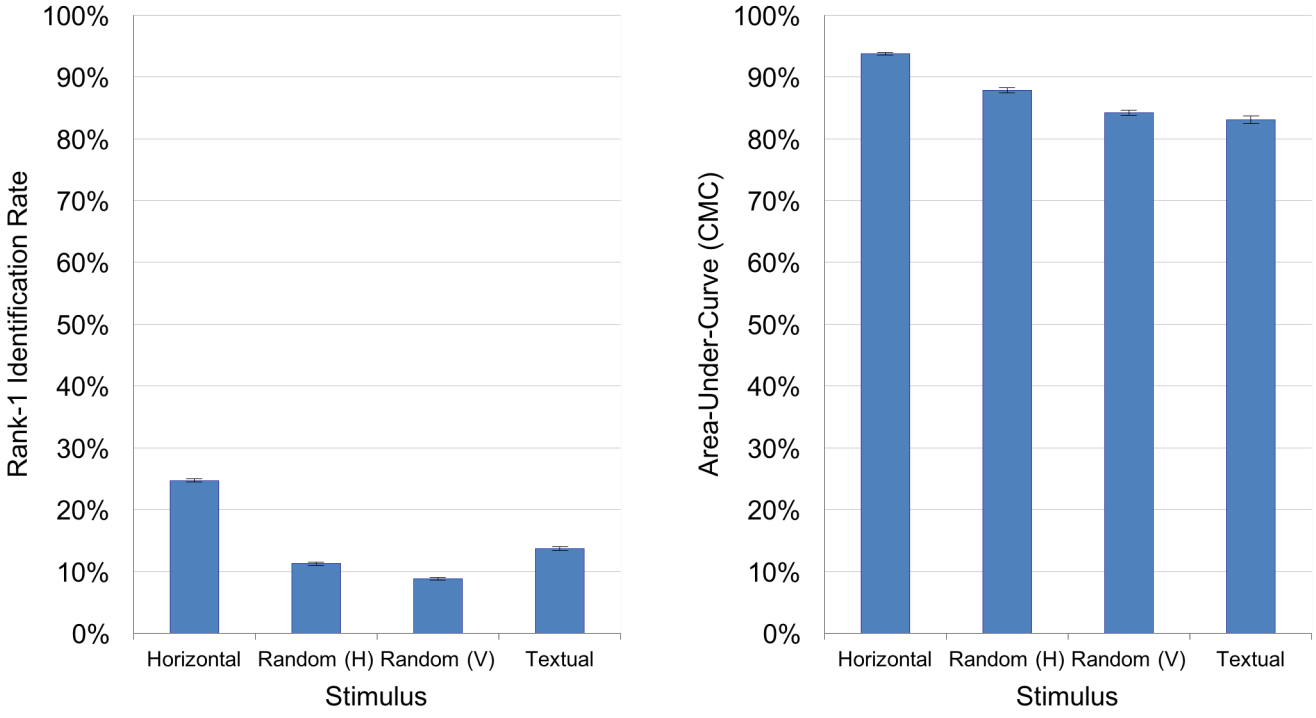


Figure 6. The effects of stimulus type on the biometric accuracy of eye movements in an identification scenario. Error bars indicate 95% confidence interval for the regression of error rates.

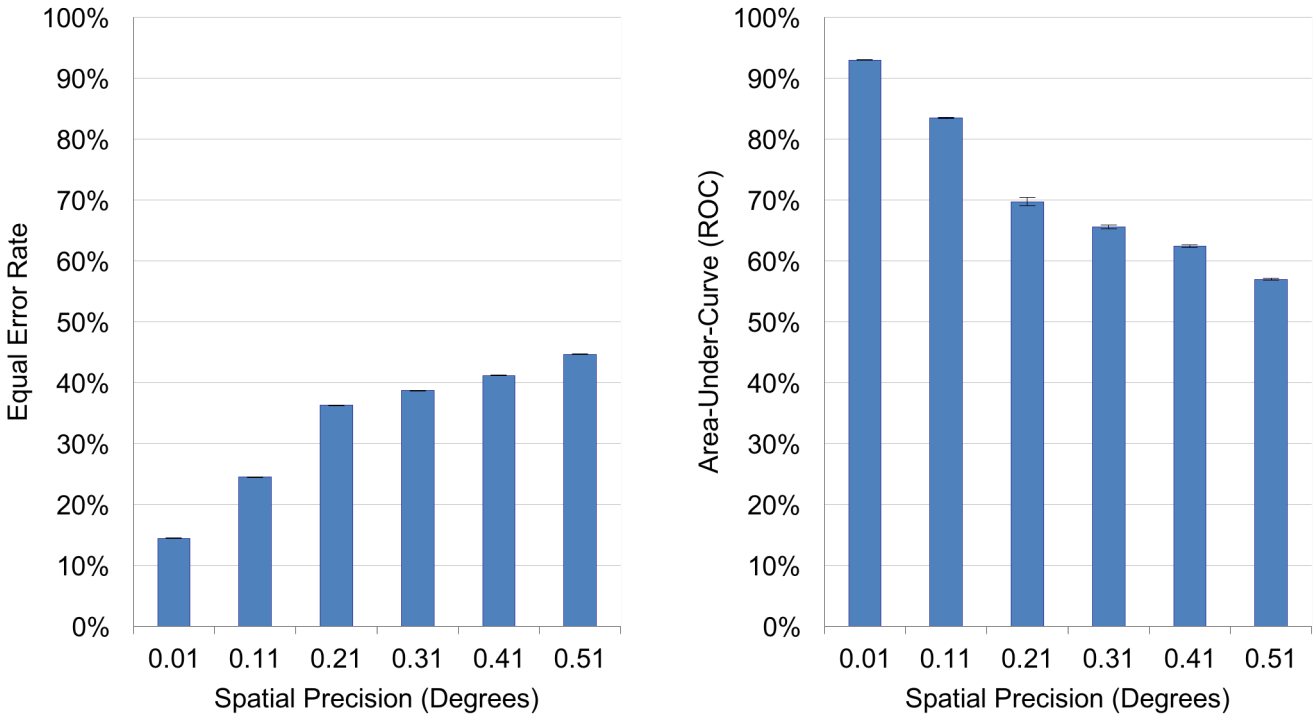


Figure 7. The effects of spatial precision on the biometric accuracy of eye movements in a verification scenario. Error bars indicate 95% confidence interval for the regression of error rates.

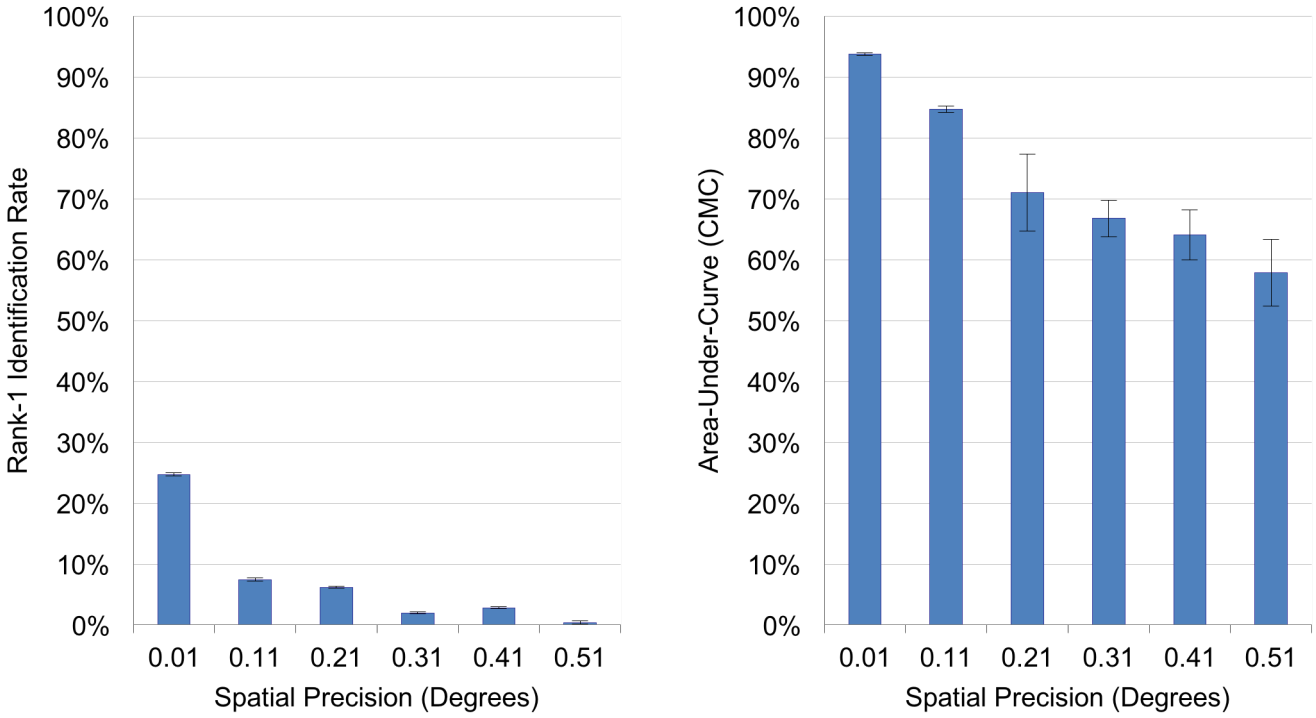


Figure 8. The effects of spatial precision on the biometric accuracy of eye movements in an identification scenario. Error bars indicate 95% confidence interval for the regression of error rates.

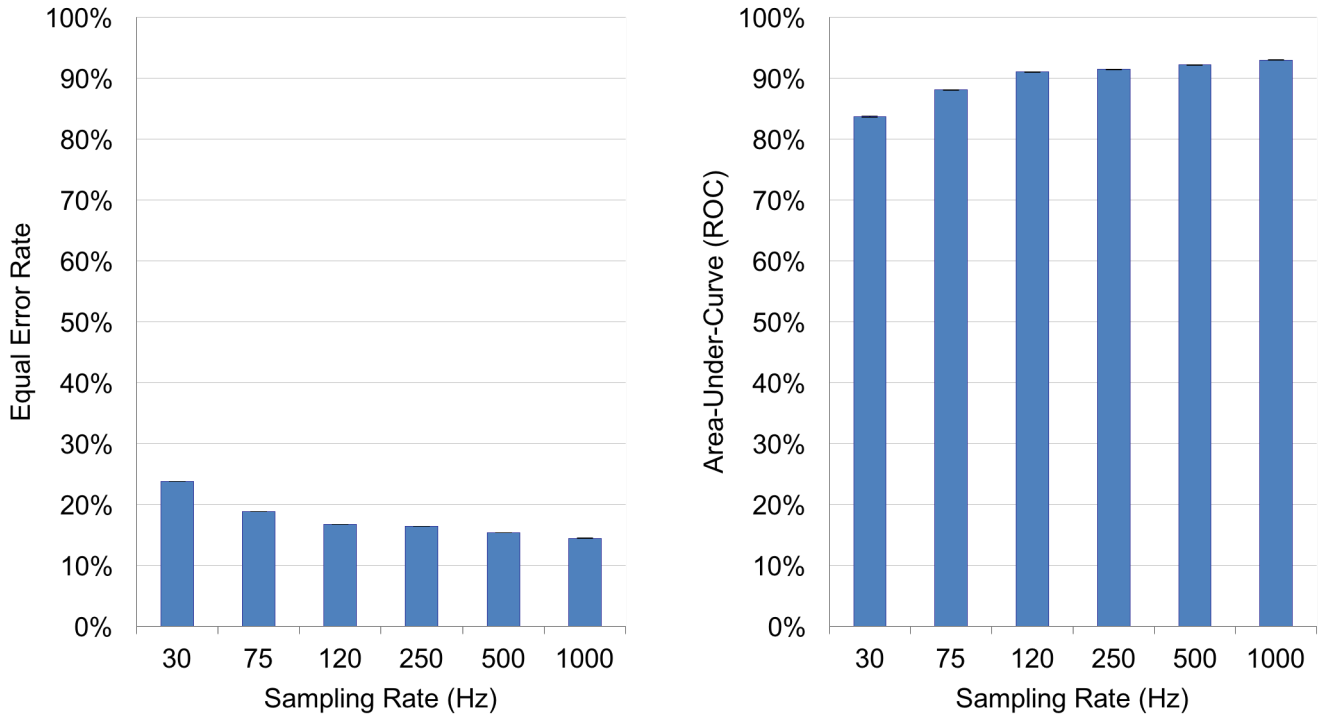


Figure 9. The effects of sampling rate on the biometric accuracy of eye movements in a verification scenario. Error bars indicate 95% confidence interval for the regression of error rates.

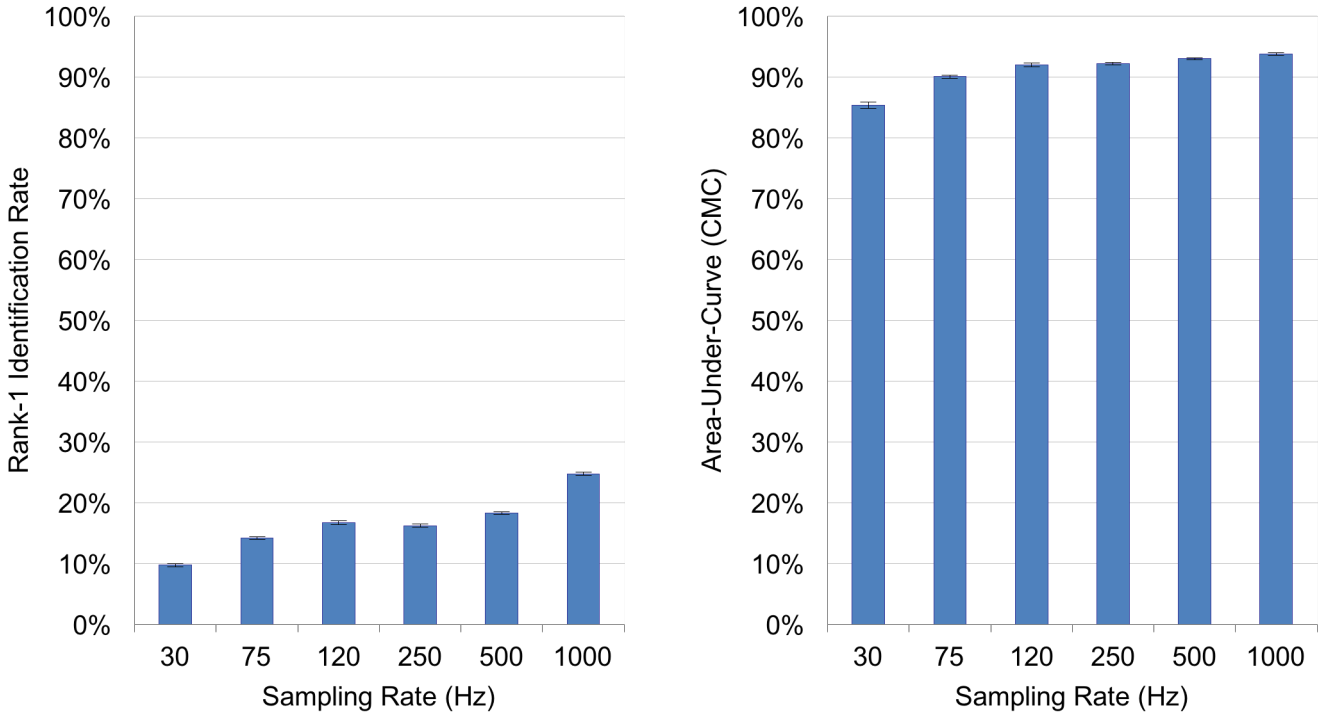


Figure 10. The effects of sampling rate on the biometric accuracy of eye movements in an identification scenario. Error bars indicate 95% confidence interval for the regression of error rates.

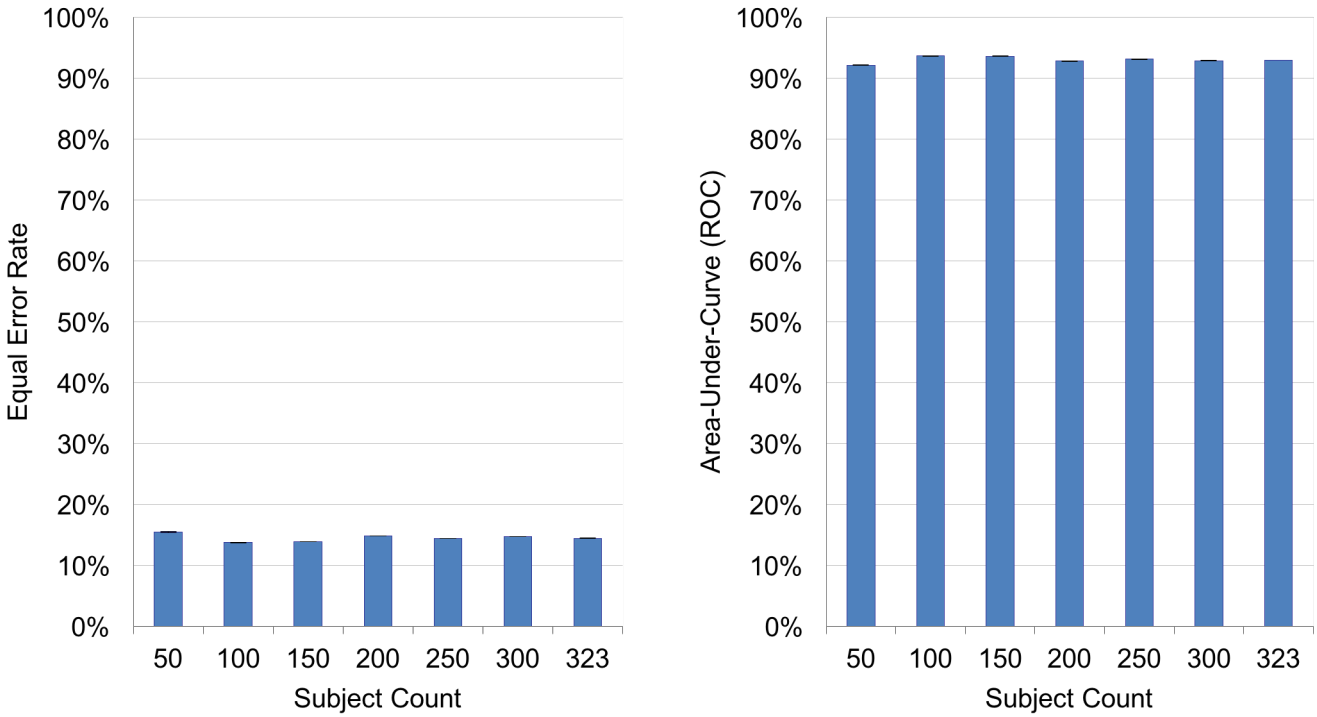


Figure 11. The effects of scaling on the biometric accuracy of eye movements in a verification scenario. Error bars indicate 95% confidence interval for the regression of error rates.

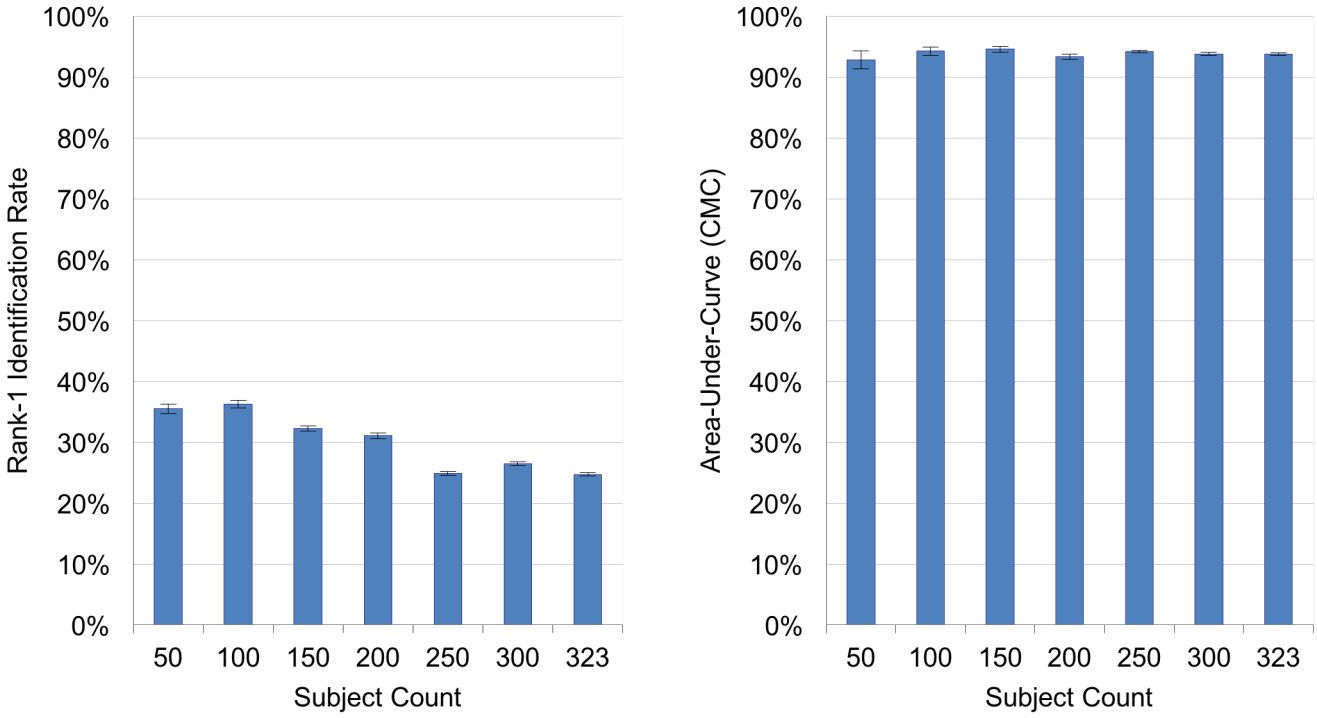


Figure 12. The effects of scaling on the biometric accuracy of eye movements in an identification scenario. Error bars indicate 95% confidence interval for the regression of error rates.

## V. Conclusion

This paper has presented an objective evaluation of the effects of environmental factors, such as stimulus presentation and eye tracking specifications, on the biometric accuracy of oculomotor plant characteristic (OPC) biometrics. Six spatial precision tiers (0.01°, 0.11°, 0.21°, 0.31°, 0.41°, 0.51°), six temporal resolution tiers (1000 Hz, 500 Hz, 250 Hz, 120 Hz, 75 Hz, 30 Hz), and three stimulus types (horizontal, random, textual) were evaluated to identify acceptable conditions under which to collect eye movement data.

The results suggest the use of eye tracking equipment with high spatial precision (i.e. close to 0.01°) and a minimum sampling rate of 30 Hz, though 120 Hz sampling rate is recommended for best performance. Further, the horizontal pattern stimulus had a clear advantage, though this may be due to the oculomotor plant model that was employed. In addition, there was little difference in the biometric accuracy produced for a subject pool of 50 compared to a subject pool of 323.

## References

[1] O. V. Komogortsev, C. D. Holland, A. Karpov, and L. R. Price, "Biometrics via Oculomotor Plant Characteristics: Impact of Parameters in Oculomotor Plant Model," ACM Transactions on Applied Perception, pp. 1-14, 2015.

[2] H. Chan and W. W. Bledsoe, "A Man-Machine Facial Recognition System; Some Preliminary Results," Panoramic Research Inc., Palo Alto, CA, USA1965.

[3] M. Turk and A. Pentland, "Eigenfaces for Recognition," Journal of Cognitive Neuroscience, vol. 3, pp. 71-86, 1991.

[4] P. J. Phillips, H. Moon, S. A. Rizvi, and P. J. Rauss, "The FERET Evaluation Methodology for Face-Recognition Algorithms," IEEE Transactions on Pattern Analysis and Machine Intelligence, vol. 22, pp. 1090-1104, 2000.

[5] S. A. Rizvi, P. J. Phillips, and H. Moon, "The FERET Verification Testing Protocol for Face Recognition Algorithms," in International Conference on Automatic Face and Gesture Recognition (FGR), Nara, Japan, 1998, pp. 48-53.

[6] W. Zhao, R. Chellappa, P. J. Phillips, and A. Rosenfeld, "Face Recognition: A Literature Survey," ACM Computing Surveys (CSUR), vol. 35, pp. 399-458, 2003.

[7] M. A. O. Vasilescu and D. Terzopoulos, "Multilinear Analysis of Images Ensembles: TensorFaces," Lectures Notes in Computer Science, vol. 2350, pp. 447-460, 2002.

[8] K. Jain, P. Flynn, and A. A. Ross, Eds., Handbook of Biometrics. Springer US, 2007.

[9] L. Wiskott, J.-M. Fellous, N. Krüger, and C. v. d. Malsburg, "Face Recognition by Elastic Bunch Graph Matching," IEEE Transactions on Pattern Analysis and Machine Intelligence, vol. 19, pp. 775-779, 1997.

[10] D. Maio, D. Maltoni, R. Cappelli, J. L. Wayman, and A. K. Jain, "FVC2004: Third Fingerprint Verification Competition.," in International Conference on Biometric Authentication, Hong Kong, China, 2004, pp. 1-7.

[11] P. Coli, G. L. Marcialis, and F. Roli, "Vitality Detection from Fingerprint Images: A Critical Survey," in Advances in Biometrics. vol. 4642, S.-W. Lee and S. Z. Li, Eds., ed: Springer Berlin, 2007, pp. 722-731.

[12] Bertillon, La Couleur de l'Iris: Masson, 1886.

[13] L. Flom and A. Safir, "Iris Recognition System," United States Patent 4,641,349, 1987.

[14] J. G. Daugman, "High Confidence Visual Recognition of Persons by a Test of Statistical Independence," IEEE Transactions on Pattern Analysis and Machine Intelligence, vol. 15, pp. 1148-1161, 1993.

[15] ITIRT, "Independent Testing of Iris Recognition Technology: Final Report," International Biometric Group, 2005.

[16] Ruiz-Albacete, P. Tome-Gonzalez, F. Alonso-Fernandez, J. Galbally, J. Fierrez, and J. Ortega-Garcia, "Direct Attacks Using Fake Images in Iris Verification," in Biometrics and Identity Management. vol. 5372, B. Schouten, N. C. Juul, A. Drygajlo, and M. Tistarelli, Eds., ed Roskilde, Denmark: Springer Berlin Heidelberg, 2008, pp. 181-190.

[17] J. Daugman, "How Iris Recognition Works," IEEE Transactions on Circuits and Systems for Video Technology, vol. 14, pp. 21-30, 2004.

[18] J. Daugman, "Probing the Uniqueness and Randomness of IrisCodes: Results From 200 Billion Iris Pair Comparisons," Proceedings of the IEEE, vol. 94, pp. 1927-1935, 2006.

[19] C. D. Holland and O. V. Komogortsev, "Complex Eye Movement Pattern Biometrics: Analyzing Fixations and Saccades," in IAPR International Conference on Biometrics (ICB), Madrid, Spain, 2013, pp. 1-8.

[20] P. Kasprowski and J. Ober, "Eye Movements in Biometrics," in European Conference on Computer Vision, Prague, Czech Republic, 2004, pp. 248-258.

[21] R. J. Leigh and D. S. Zee, The Neurology of Eye Movements, 4 ed. Oxford, NY, USA: Oxford University Press, 2006.

[22] O. V. Komogortsev and A. Karpov, "Liveness Detection via Oculomotor Plant Characteristics: Attack of Mechanical Replicas," in IEEE/IAPR International Conference on Biometrics (ICB), Madrid, Spain, 2013, pp. 1-8.

[23] J. S. Agustin, H. Skovsgaard, J. P. Hansen, and D. W. Hansen, "Low-cost Gaze Interaction: Ready to Deliver the Promises," in Conference on Human Factors in Computing, Boston, MA, USA, 2009, pp. 4453-4458.

[24] T. Duchowski, Eye Tracking Methodology: Theory and Practice, 2 ed. London, UK: Springer-Verlag, 2007.

[25] D. Noton and L. W. Stark, "Scanpaths in Eye Movements during Pattern Perception," Science, vol. 171, pp. 308-311, 1971.

[26] K. Rayner, "Eye Movements in Reading and Information Processing: 20 Years of Research," Psychological Bulletin, vol. 124, pp. 372-422, 1998.

[27] B. S. Schnitzer and E. Kowler, "Eye Movements during Multiple Readings of the Same Text," Vision Research, vol. 46, pp. 1611-1632, 2005.

[28] R. Bednarik, T. Kinnunen, A. Mihaila, and P. Fränti, "Eye-Movements as a Biometric," in Image Analysis, H.

Kalviainen, J. Parkkinen, and A. Kaarna, Eds., ed: Springer Berlin Heidelberg, 2005, pp. 780-789.
[29] D. L. Silver and A. J. Biggs, "Keystroke and Eye-Tracking Biometrics for User Identification," in International Conference on Artificial Intelligence (ICAI), Las Vegas, NV, USA, 2006, pp. 344-348.
[30] C. D. Holland and O. V. Komogortsev, "Biometric Identification via Eye Movement Scanpaths in Reading," in International Joint Conference on Biometrics (IJCB), Washington, D.C., 2011, pp. 1-8.
[31] O. V. Komogortsev, A. Karpov, L. R. Price, and C. R. Aragon, "Biometric Authentication via Oculomotor Plant Characteristics," in International Conference on Biometrics (ICB), New Delhi, India, 2012, pp. 1-8.
[32] O. V. Komogortsev and C. D. Holland, "Biometric Authentication via Complex Oculomotor Behavior," in International Conference on Biometrics: Theory, Applications and Systems (BTAS), Washington, DC, USA, 2013, pp. 1-8.
[33] C. Quaia and L. M. Optican, "Dynamic Eye Plant Models and the Control of Eye Movements," Strabismus, vol. 11, pp. 17-31, 2003.
[34] D. R. Wilkie, Muscle, 2 ed. London: Arnold, 1970.
[35] T. Bahill, "Development, Validation, and Sensitivity Analyses of Human Eye Movement Models," Critical Reviews in Bioengineering, vol. 4, pp. 311-355, 1980.
[36] O. V. Komogortsev, C. D. Holland, U. K. S. Jayarathna, and A. Karpov, "2D Linear Oculomotor Plant Mathematical Model: Verification and Biometric Applications," ACM Transactions on Applied Perception, vol. 10, pp. 1-18, 2013.
[37] J. C. Lagarias, J. A. Reeds, M. H. Wright, and P. E. Wright, "Convergence Properties of the Nelder-Mead Simplex Method in Low Dimensions," SIAM Journal of Optimization, vol. 9, pp. 112-147, 1998.
[38] O. V. Komogortsev and U. K. S. Jayarathna, "2D Oculomotor Plant Mathematical Model for Eye Movement Simulation," in International Conference on BioInformatics and BioEngineering (BIBE), Athens, Greece, 2008, pp. 1-8.
[39] O. V. Komogortsev and J. I. Khan, "Eye Movement Prediction by Kalman Filter with Integrated Linear Horizontal Oculomotor Plant Mechanical Model," in Eye Tracking Research & Applications (ETRA) Symposium, Savannah, GA, USA, 2008, pp. 229-236.
[40] M. Nyström, R. Andersson, K. Holmqvist, and J. van de Weijer, “The Influence of Calibration Method and Eye Physiology on Eyetracking Data Quality,” Behavior Research Methods, vol. 45, pp. 272-288, 2013.
[41] SR Research. EyeLink 1000 Eye Tracker. Available: http://www.sr-research.com/
[42] SR Research. EyeLink 1000 User Manual. Available: http://www.sr-research.com/
[43] D. D. Salvucci and J. H. Goldberg, "Identifying Fixations and Saccades in Eye-tracking Protocols," in Eye Tracking Research & Applications Symposium, Palm Beach Gardens, FL, USA, 2000, pp. 71-78.
[44] O. V. Komogortsev, D. V. Gobert, U. K. S. Jayarathna, D. H. Koh, and S. M. Gowda, "Standardization of Automated Analyses of Oculomotor Fixation and Saccadic Behaviors," IEEE Transactions on Biomedical Engineering, vol. 57, pp. 2635-2645, 2010.
[45] C. Smit, A. J. v. Opstal, and J. A. M. v. Gisbergen, "Component Stretching in Fast and Slow Oblique Saccades in the Human," Experimental Brain Research, vol. 81, pp. 325-334, 1990.
[46] A. Bahill and L. Stark, “Oblique Saccadic Eye Movements: Independence of Horizontal and Vertical Channels,” Archive of Ophthalmology, vol. 95, pp. 1258-1261, 1977.
[47] G. E. Grossman and D. A. Robinson, "Ambivalence in Modelling Oblique Saccades," Biological Cybernetics, vol. 58, pp. 13-18, 2004.
[48] K. Holmqvist, M. Nyström, and F. Mulvey, “Eye Tracker Data Quality: What It Is and How to Measure It,” in Proceedings of the Symposium on Eye Tracking Research and Applications (ETRA), Santa Barbara, CA, USA, 2012, pp. 45-52.